

Learning Laplacian Eigenvectors: a Pre-training Method for Graph Neural Networks

Howard Dai^{1,*} Nyambura Njenga^{2,*}
 Benjamin Whitsett³ Catherine Ma⁴ Darwin Deng¹ Sara de Ángel¹ Alexandre Van Tassel¹
 Siddharth Viswanath¹ Ryan Pellico^{5,†} Ian Adelstein^{1,†} Smita Krishnaswamy^{1,†}

¹Yale University ²Georgia Institute of Technology ³Kalamazoo College

⁴Pomona College ⁵Trinity College

*co-first authors [†]co-senior authors

Correspondence: smitta.krishnaswamy@yale.edu

Abstract

We propose a novel framework for pre-training Graph Neural Networks (GNNs) by inductively learning Laplacian eigenvectors. Traditional Message Passing Neural Networks (MPNNs) often struggle to capture global and regional graph structure due to over-smoothing risk as network depth increases. Because the low-frequency eigenvectors of the graph Laplacian matrix encode global information, pre-training GNNs to predict these eigenvectors encourages the network to naturally learn large-scale structural patterns over each graph. Empirically, we show that models pre-trained via our framework outperform baseline models on a variety of graph structure-based tasks. While most existing pre-training methods focus on domain-specific tasks like node or edge feature reconstruction, our self-supervised pre-training framework is structure-based and highly flexible. Eigenvector-learning can be applied to all graph-based datasets, and can be used with synthetic features when task-specific data is sparse.

1 Introduction

Graph Neural Networks (GNNs) have become a powerful tool in node and graph representation learning, with successful applications across domains ranging from biomedicine [1–4] to social networks [5]. However, traditional message passing GNNs often struggle to capture the global and regional structure of the graph, primarily due to the risk of over-smoothing as network depth increases [6, 7]. One promising solution is to pre-train GNNs on structure-aware tasks [4]. In particular, pre-training a GNN to produce the low-frequency eigenvectors of the graph Laplacian enables it to learn global patterns within the data. These low-frequency eigenvectors capture global and regional structure; by training the GNN to produce the lower frequency components, we encourage it to focus on the larger-scale structure of the graph. The pre-trained model can then be fine-tuned on other downstream, context-aware tasks, or its embeddings can be used as positional encodings for Graph Transformer networks. Moreover, since Laplacian eigenvector learning is entirely structure-based, it can be used as a training task for transfer learning and graph foundation models.

While some structure-informed pre-training tasks have been proposed, the majority are tailored to specific domains and rely on access to informative node features [2, 3]. Common strategies include context-prediction and motif or cluster prediction [2–4]. Existing domain-agnostic pre-training strategies also suffer from over-smoothing, as they rely solely on deep message passing GNNs [1–3] with basic node-wise prediction heads. This highlights the need for an alternative prediction head that can naturally capture and synthesize long-range structural information.

Our main contributions are as follows:

1. We introduce Laplacian eigenvector-learning as a structure-based pre-training task for GNNs.

2. We introduce a global MLP head that enables long-range interaction between vertices within the graph, improving the effectiveness of eigenvector-based pre-training.
3. We demonstrate that our pre-training framework provides performance improvements over baseline models on various structure-based downstream applications.

2 Background and Notation

The Laplacian L of a graph G is defined as:

$$L = D - A$$

where D is the diagonal degree matrix and A is the unnormalized adjacency matrix of G .

Let $\lambda_1, \lambda_2, \dots, \lambda_k$ denote the k lowest eigenvalues of L in nondecreasing order. Let $\psi_1, \psi_2, \dots, \psi_k$ denote the corresponding eigenvectors.

By Courant-Fischer, the eigenvectors of L (and the eigenvectors of any Hermitian matrix) can be expressed as the following iterative optimization problem:

$$\psi_k \in \underset{\substack{\|x\|=1 \\ x \perp \psi_1, \dots, \psi_{k-1}}}{\operatorname{argmin}} x^\top L x.$$

The term $\frac{x^\top L x}{x^\top x}$ is known as the Rayleigh quotient; because we normalize our predicted eigenvectors, we simply treat this as $x^\top L x$.

3 Method

3.1 Model Architecture

Base GNN: The base GNN model takes in a graph with augmented node features and generates learned node representations via neighborhood message passing and update steps. Any GNN architecture may be selected as the base model to fit the needs of the dataset and downstream application.

Graph-level MLP: We concatenate the node-wise output of the base GNN model to form a graph-level aggregated representation. We then pass the aggregated vector through an MLP model to produce the low-frequency Laplacian eigenvectors. Concatenating the node embeddings prior to applying the MLP allows the model to learn relationships between distant nodes without risking over-smoothing.

Previous eigenvector-learning methods use a node-wise MLP head, processing each node’s eigencoordinates independently based on their learned hidden embedding [1, 8, 9].

3.2 Node Feature Augmentation

To provide the model with additional structural information, we augment node features with structure-based embeddings. We propose two kinds of embeddings: **(1) wavelet positional embeddings**, which encode relative positional information between nodes, and **(2) diffused dirac embeddings**, which encode local connectivity structures around each node. Both embeddings use the random walk matrix, and capture local aggregate information on each node. We discuss these embeddings in detail in A.4.

3.3 Loss function

We minimize a weighted sum of two loss functions: **(1) eigenvector loss** and **(2) energy loss**.

Let \hat{U} denote a matrix of column vectors \hat{u}_i , where each \hat{u}_i denotes the i th predicted eigenvector.

Eigenvector loss, used in [10], measures the difference between each $L\hat{u}_i$ and $\lambda_i\hat{u}_i$:

$$\mathcal{L}_{eigvec} = \frac{1}{k} \|(L\hat{U} - \hat{U}\Lambda_k)\|$$

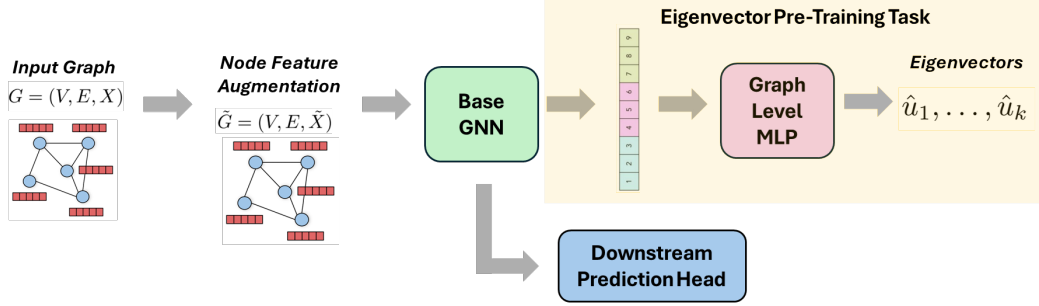


Figure 1: Visual illustration of Laplacian Eigenvector GNN pre-training framework.

Energy loss, used in [8, 9, 11], aims to minimize the sum of Rayleigh quotients:

$$\mathcal{L}_{energy} = \frac{1}{k} \text{Tr}(\hat{U}^\top L \hat{U})$$

To ensure the model does not output k copies of the trivial eigenvector, we impose orthogonality on the final outputs of the model via QR decomposition, as proposed in [8].

We show that our loss functions satisfy necessary sign and basis invariances. Full proofs can be found in A.3.

3.4 Pre-Training Algorithm

Algorithm 1 Eigenvector Learning

Require: Graph $G = (V, E)$; augmented node features $\tilde{X} = \{\tilde{x}_j\}$; Base GNN

Ensure: Output Pre-trained GNN model, k lowest-frequency eigenvectors

- 1: **for** $i < \text{Pre-Training Epochs}$ **do**
 - 2: $\tilde{z}_0, \dots, \tilde{z}_n \leftarrow \text{BASEGNN}(G, \tilde{X})$
 - 3: $\tilde{Z} \leftarrow [\tilde{z}_1, \dots, \tilde{z}_n] \in \mathbb{R}^{n \times d}$
 - 4: $\tilde{U} \leftarrow \text{MLP}(\tilde{Z})$
 - 5: $\hat{U} = \text{QR}(\tilde{U})$
 - 6: $\text{Loss} = \alpha \cdot \text{ENERGYLOSS}(\hat{U}) + \beta \cdot \text{EIGVECLoss}(\hat{U})$
 - 7: Back-propagate Loss, update model weights
 - 8: **end for**
 - 9: **return** BASEGNN
-

4 Experimental Results

4.1 Standalone pre-training

We pre-train a standard Graph Isomorphism Network (GIN) [12] on the eigenvector-learning task with the graph-level MLP head. Once the model has been pre-trained, we replace the graph-level MLP head with a downstream prediction MLP and fine-tune model weights. We evaluate our pre-training framework on two molecular datasets, ZINC-12k [13] and QM9 [14]. We record results of our experiments in Table 1. On 7 of 8 total targets, eigenvector pre-training substantially improves downstream performance.

4.2 Augmenting existing pre-training method

We augment the existing molecular pre-training methods proposed in [3] with eigenvector-learning. In particular, [3] proposes node-level pre-training tasks (context prediction and masking) on ZINC15 [13], followed by a graph-level supervised pre-training task on ChEMBL [15, 16]. We augment the graph-level supervised pre-training step by adding an additional MLP head to predict eigenvectors, and we evaluate on five downstream datasets based on [4].

Detailed results are shown in Table 2. Eigenvector-learning consistently improves performance for the masking pre-training pipeline, but achieves mixed results on the context prediction pipeline. Notably, performance for the masking pipeline was increased for all five datasets when performing eigenvector pre-training with the graph-level MLP head.

4.3 Augmenting existing graph structural encoder

We modify Graph Positional and Structural Encoder (GPSE) [1]. While GPSE already incorporates eigenvector-learning by including Laplacian positional encodings (LapPE) as a prediction target, GPSE uses MAE and cosine similarity loss on the absolute value of each eigenvector and a node-wise prediction head for every node property. We replace GPSE’s eigenvector-learning component with our own, using a separate MLP head and eigenvector loss. We keep all other GPSE model settings the same.

Following [1], we pre-train our modified GPSE model on MolPCBA [17]. We evaluate the effectiveness of these encodings by training both the Transformer model GPS [18] and a standard GIN, augmented with these encodings, on the downstream molecule property prediction task for the ZINC 12k [13] subset.

We report results on the effectiveness of these new learned encodings in Table 3. Modified eigenvector-learning with a graph-level MLP improves performance on downstream performance for both the GIN and GPS models, with our graph-level GPS+GPSE+ configuration achieving SOTA performance over all model and encoding configurations tested in [1]. We also demonstrate that our choice of loss function is crucial for eigenvector-learning in A.7.

Table 3: Test MAE (\downarrow) performance on ZINC (12k subset) dataset when **augmenting a graph structural encoder**. All results using no structural encoder or the base GPSE are taken directly from [1]. GPSE+ refers to GPSE with modified eigenvector-learning (our method). Our experimental results are averaged over three seeds.

Base model	Structural encoder	MLP Head	MAE
GPS	GPSE+	Graph-level	0.0629 \pm 0.0016
	GPSE+	Node-wise	0.0663 \pm 0.0024
	GPSE	-	0.0648 \pm 0.0030
	None	-	0.118 \pm 0.005
GIN	GPSE+	Graph-level	0.1231 \pm 0.0026
	GPSE+	Node-wise	0.1299 \pm 0.0010
	GPSE	-	0.124 \pm 0.002
	None	-	0.285 \pm 0.004

5 Limitations and Future Work

There are several promising future directions toward improving the Laplacian eigenvector pre-training framework. We have demonstrated the effectiveness of the framework for pre-training and fine-tuning a GNN on the same dataset, or on domain-related datasets. However, we are yet to explore the effectiveness of eigenvector pre-training as a *transfer learning* framework.

Further, the practical implementation of the graph-level MLP requires adding padding to the concatenated node embeddings to accommodate for graphs of differing sizes. This creates an additional challenge for the MLP to learn meaningful relationships between the individual node embeddings within the graph-level vector. One could explore other ways of creating a rich graph-level representation while avoiding this challenge.

References

- [1] Semih Cantürk, Renming Liu, Olivier Lapointe-Gagné, Vincent Létourneau, Guy Wolf, Dominique Beaini, and Ladislav Rampásek. Graph positional and structural encoder. In *Forty-first International Conference on Machine Learning*, 2023. 1, 2, 4, 10, 11

Table 1: Test MAE (\downarrow) performance comparison on ZINC (single metric) and QM9 (first seven target properties).

Model	ZINC			QM9				
	Penalized log p	μ	α	$\varepsilon_{\text{HOMO}}$	$\varepsilon_{\text{LUMO}}$	Δ_{ε}	$\langle R^2 \rangle$	ZPVE
Pre-Trained GIN	0.353	0.484	0.489	0.00353	0.00371	0.00513	28.103	0.000477
Baseline GIN	0.438	0.472	1.132	0.00386	0.00399	0.00562	50.909	0.002400

Table 2: Test ROC-AUC (%, \uparrow) performance on 5 molecular prediction tasks when **augmenting an existing pre-training method** on a GIN base model. *Sup.* refers to the original supervised pre-training as implemented in [3], and *Sup. +* refers to supervised training with additional eigenvector-learning (our method). Results for *no pre-training* are taken directly from [4]. All methods are tuned over seven learning rates and averaged over three seeds.

Dataset		BACE	BBBP	Tox21	ToxCast	SIDER
Pretrain method	MLP Head					
ContextPred, Sup. +	Graph-level	79.62 \pm 3.63	70.76 \pm 1.64	77.94 \pm 0.11	66.13 \pm 0.34	60.05 \pm 0.99
ContextPred, Sup. +	Node-wise	75.87 \pm 3.11	68.74 \pm 1.07	78.86 \pm 0.06	63.78 \pm 0.32	59.83 \pm 0.53
ContextPred, Sup.	-	84.98 \pm 1.28	68.25 \pm 0.48	77.44 \pm 0.19	64.01 \pm 0.81	62.87 \pm 0.89
Masking, Sup. +	Graph-level	80.71 \pm 3.84	68.33 \pm 0.89	<i>79.09 \pm 0.25</i>	<i>65.96 \pm 0.20</i>	<i>62.41 \pm 1.77</i>
Masking, Sup. +	Node-wise	<i>81.02 \pm 1.67</i>	<i>69.94 \pm 1.76</i>	79.33 \pm 0.41	65.14 \pm 0.44	59.38 \pm 1.11
Masking, Sup.	-	75.42 \pm 2.64	67.36 \pm 4.60	78.33 \pm 0.24	64.88 \pm 0.82	61.6 \pm 1.78
No pre-training	-	75.77 \pm 4.29	69.62 \pm 1.05	75.52 \pm 0.67	63.67 \pm 0.32	59.07 \pm 1.13

- [2] Pengwei Yan, Kaisong Song, Zhuoren Jiang, Yangyang Kang, Tianqianjin Lin, Changlong Sun, and Xiaozhong Liu. Empowering dual-level graph self-supervised pretraining with motif discovery. In *Proceedings of the AAAI Conference on Artificial Intelligence*, volume 38, pages 9223–9231, 2024. 1
- [3] Weihua Hu, Bowen Liu, Joseph Gomes, Marinka Zitnik, Percy Liang, Vijay Pande, and Jure Leskovec. Strategies for pre-training graph neural networks. In *International Conference on Learning Representations*, 2019. 1, 3, 5, 10
- [4] Ruoxi Sun, Hanjun Dai, and Adams Wei Yu. Does gnn pretraining help molecular representation? *Advances in Neural Information Processing Systems*, 35:12096–12109, 2022. 1, 3, 5, 10
- [5] Wenqi Fan, Yao Ma, Qing Li, Yuan He, Eric Zhao, Jiliang Tang, and Dawei Yin. Graph neural networks for social recommendation. In *The world wide web conference*, pages 417–426, 2019. 1
- [6] Nicolas Keriven. Not too little, not too much: a theoretical analysis of graph (over) smoothing. *Advances in Neural Information Processing Systems*, 35:2268–2281, 2022. 1
- [7] Lingxiao Zhao and Leman Akoglu. Pairnorm: Tackling oversmoothing in gnns. In *International Conference on Learning Representations*. 1
- [8] Uri Shaham, Kelly Stanton, Henry Li, Ronen Basri, Boaz Nadler, and Yuval Kluger. Spectralnet: Spectral clustering using deep neural networks. In *International Conference on Learning Representations*, 2018. 2, 3, 7
- [9] Vijay Prakash Dwivedi, Anh Tuan Luu, Thomas Laurent, Yoshua Bengio, and Xavier Bresson. Graph neural networks with learnable structural and positional representations. In *International Conference on Learning Representations*, 2021. 2, 3, 7
- [10] Gal Mishne, Uri Shaham, Alexander Cloninger, and Israel Cohen. Diffusion nets. *Applied and Computational Harmonic Analysis*, 47(2):259–285, 2019. 2
- [11] Yixuan Ma and Kun Zhan. Self-contrastive graph diffusion network. In *Proceedings of the 31st ACM International Conference on Multimedia*, pages 3857–3865, 2023. 3, 7
- [12] Keyulu Xu, Weihua Hu, Jure Leskovec, and Stefanie Jegelka. How powerful are graph neural networks? In *International Conference on Learning Representations*, 2019. 3
- [13] Teague Sterling and John J Irwin. Zinc 15–ligand discovery for everyone. *Journal of chemical information and modeling*, 55(11):2324–2337, 2015. 3, 4
- [14] Raghunathan Ramakrishnan, Pavlo O Dral, Matthias Rupp, and O Anatole Von Lilienfeld. Quantum chemistry structures and properties of 134 kilo molecules. *Scientific data*, 1(1):1–7, 2014. 3
- [15] Andreas Mayr, Günter Klambauer, Thomas Unterthiner, Marvin Steijaert, Jörg K Wegner, Hugo Ceulemans, Djork-Arné Clevert, and Sepp Hochreiter. Large-scale comparison of machine learning methods for drug target prediction on chembl. *Chemical science*, 9(24):5441–5451, 2018. 3

- [16] Anna Gaulton, Louisa J Bellis, A Patricia Bento, Jon Chambers, Mark Davies, Anne Hersey, Yvonne Light, Shaun McGlinchey, David Michalovich, Bissan Al-Lazikani, et al. ChEMBL: a large-scale bioactivity database for drug discovery. *Nucleic acids research*, 40(D1):D1100–D1107, 2012. 3
- [17] Weihua Hu, Matthias Fey, Marinka Zitnik, Yuxiao Dong, Hongyu Ren, Bowen Liu, Michele Catasta, and Jure Leskovec. Open graph benchmark: Datasets for machine learning on graphs. *Advances in neural information processing systems*, 33:22118–22133, 2020. 4
- [18] Ladislav Rampásek, Michael Galkin, Vijay Prakash Dwivedi, Anh Tuan Luu, Guy Wolf, and Dominique Beaini. Recipe for a general, powerful, scalable graph transformer. *Advances in Neural Information Processing Systems*, 35:14501–14515, 2022. 4
- [19] Govindan Subramanian, Bharath Ramsundar, Vijay Pande, and Rajiah Aldrin Denny. Computational modeling of β -secretase 1 (bace-1) inhibitors using ligand based approaches. *Journal of chemical information and modeling*, 56(10):1936–1949, 2016. 10
- [20] Ines Filipa Martins, Ana L Teixeira, Luis Pinheiro, and Andre O Falcao. A bayesian approach to in silico blood-brain barrier penetration modeling. *Journal of chemical information and modeling*, 52(6):1686–1697, 2012. 10
- [21] Andreas Mayr, Günter Klambauer, Thomas Unterthiner, and Sepp Hochreiter. Deeptox: toxicity prediction using deep learning. *Frontiers in Environmental Science*, 3:80, 2016. 10
- [22] Ann M Richard, Richard S Judson, Keith A Houck, Christopher M Grulke, Patra Volarath, Inthirany Thillainadarajah, Chihae Yang, James Rathman, Matthew T Martin, John F Wambaugh, et al. Toxcast chemical landscape: paving the road to 21st century toxicology. *Chemical research in toxicology*, 29(8):1225–1251, 2016. 10
- [23] Michael Kuhn, Ivica Letunic, Lars Juhl Jensen, and Peer Bork. The sider database of drugs and side effects. *Nucleic acids research*, 44(D1):D1075–D1079, 2016. 10

A Appendix

A.1 Full eigenvector pre-training pipeline

We provide a broad algorithmic outline of eigenvector pre-training process in Algorithm 2.

Algorithm 2 Structure-Informed Graph Pre-training Framework

Input: Graph $G = (V, E)$; node features $X = \{x_j\}$; training labels Y ; untrained Base GNN; untrained Downstream Prediction Head

Output: Trained Base GNN and Downstream Prediction Head

```

1:  $\tilde{X} \leftarrow \text{AUGMENTFEATURES}(G, X)$ 
2:  $\text{BASEGNN} \leftarrow \text{EIGVECPRETRAIN}(G, \tilde{X}, \text{BASEGNN})$ 
3: for  $i < \text{Fine-tuning Epochs}$  do
4:    $\vec{z}_0, \dots, \vec{z}_n \leftarrow \text{BASEGNN}(G, \tilde{X})$ 
5:    $\vec{Z} \leftarrow [\vec{z}_1, \dots, \vec{z}_n]$ 
6:    $\hat{Y} \leftarrow \text{DOWNSTREAMHEAD}(\vec{Z})$ 
7:    $\text{Loss} = \text{LOSSCRITERION}(\hat{Y}, Y)$ 
8:   Backpropagate Loss, update model weights
9: end for
10: return BASEGNN, DOWNSTREAMHEAD
    
```

A.2 Loss function

Eigenvector loss, per-vector form:

$$\mathcal{L}_{\text{eigvec}} = \frac{1}{k} \sum_{i=1}^k \|L\hat{u}_i - \lambda_i \hat{u}_i\|$$

Eigenvector loss, matrix form:

$$\mathcal{L}_{eigvec} = \frac{1}{k} \|(L\hat{U} - \hat{U}\Lambda_k)\|$$

Energy loss, per-vector form:

$$\mathcal{L}_{energy} = \frac{1}{k} \sum_{i=1}^k \hat{u}_i^\top L \hat{u}_i$$

Energy loss, matrix form:

$$\mathcal{L}_{energy} = \frac{1}{k} \text{Tr}(\hat{U}^\top L \hat{U})$$

Energy loss is order-invariant and rotation invariant (see A.3); for applications in clustering, this is reasonable. However, we would like the model to learn the eigenvectors in their specific order, so we also define **absolute energy loss**, matching the Rayleigh quotient with the ground-truth eigenvalue:

$$\mathcal{L}_{energy_abs} = \frac{1}{k} \sum_{i=1}^k |\hat{u}_i^\top L \hat{u}_i - \lambda_i|$$

This can be written as, in matrix form:

$$\mathcal{L}_{energy_abs} = \frac{1}{k} \text{Tr}|\hat{U}^\top L \hat{U} - \Lambda_k|$$

In practice, we do not show any results using absolute energy loss, and instead linearly combine energy loss with eigenvector loss to avoid order and rotation invariance. However, absolute energy loss remains an interesting avenue to explore.

A.2.1 Orthogonality

To ensure the model does not output k copies of the trivial eigenvector, we must give the model orthogonality constraints on the output vectors. There are again two reasonable choices here: **(1) forced orthogonality** and **(2) orthogonality loss**.

Forced orthogonality, used in [8], imposes orthogonality on the final outputs of the model via QR decomposition. In other words, if \hat{U}' is the initial output to the model, Q is an $n \times k$ matrix with orthonormal columns, and R is a $k \times k$ upper triangular matrix, then we achieve the final output \hat{U} as such:

$$\begin{aligned} QR &= \hat{U}' \\ \hat{U} &= Q \end{aligned}$$

Orthogonality loss, used in [9–11] imposes a softer constraint, encouraging orthogonality by penalizing the model for producing pairwise similar vectors. This can be written as:

$$\mathcal{L}_{ortho} = \frac{1}{k} \|\hat{U}^\top \hat{U} - I\|$$

Based on preliminary testing, we found that forced orthogonality improved performance on the eigenvector-learning, and thus use forced orthogonality in all of our experiments.

A.3 Energy and eigenvector losses are sign and basis invariant

A.3.1 Definition of basis invariance

Consider any eigenspace spanned by ground truth eigenvectors $[\psi_j, \psi_{j+1}, \dots, \psi_{j+k-1}] = V$. Also recall that, by Spectral Theorem, we can decompose any vector u into a linear combination of all eigenvectors:

$$u = \sum_{i=1}^n c_i \psi_i$$

Then a loss function is basis invariant if any rotation of the projected component $VV^\top u$ does not change the loss incurred by u . In other words, u gets to arbitrarily “choose” with what basis it wants to express its $VV^\top u$ component. Sign invariance is a special case of basis invariance, where changing sign is equivalent to rotating over a one-dimensional subspace (note that this is slightly stronger than the most apparent form of sign invariance, where we would say $\mathcal{L}(u) = \mathcal{L}(-u)$; instead, we can flip any component $c_i \psi_i$ of u when decomposed in terms of eigenvectors).

Definition 1 (Basis invariance). *Consider an eigenspace spanned by ground truth eigenvectors $[\psi_j, \psi_{j+1}, \dots, \psi_{j+k-1}] = \Psi \in \mathbb{R}^{n \times k}$. Consider an eigenspace rotation R_Ψ defined as such:*

$$R_\Psi = \Psi A \Psi^\top + (I_n - \Psi \Psi^\top), A \in \text{SO}(k)$$

A loss function $\mathcal{L}(u)$ is basis invariant if, for all such $\Psi, R_\Psi, u \in \mathbb{R}^n$, we have:

$$L(u) = L(R_\Psi u)$$

A.3.2 Proofs

Lemma 1 (Energy loss is basis invariant). *For any R_Ψ and a single eigenvector prediction $u \in \mathbb{R}^n$, we have:*

$$u^\top L u = (R_\Psi u)^\top L (R_\Psi u)$$

Proof. First note that R_Ψ is orthogonal; the set of all R_Ψ describes a subset of $\text{SO}(k)$ where only the k basis vectors in Ψ are rotated. Thus, we have $R_\Psi^\top R_\Psi = I$.

In addition, because Ψ is an eigenspace, all columns are eigenvectors with a shared eigenvalue λ . Then we have:

$$R_\Psi L = \Psi A \Psi^\top L + L - \Psi \Psi^\top L = \lambda \Psi A \Psi^\top + L - \lambda \Psi \Psi^\top = L \Psi A \Psi^\top + L - L \Psi \Psi^\top = L R_\Psi$$

Then we have:

$$R_\Psi^\top L R_\Psi = R_\Psi^\top R_\Psi L = L$$

Thus, for any u , we have:

$$u^\top L u = u^\top R_\Psi^\top L R_\Psi u = (R_\Psi u)^\top L (R_\Psi u)$$

□

Lemma 2 (Eigenvector loss is basis invariant). *For any R_Ψ and a single eigenvector prediction $u \in \mathbb{R}^n$ and ground truth eigenvalue λ , we have:*

$$\|Lu - \lambda u\| = \|L(R_\Psi u) - \lambda(R_\Psi u)\|$$

Proof. We know, from our proof above in Lemma 1, that $R_\Psi L = L R_\Psi$. Because $R_\Psi \in \text{SO}(k)$, we have $\|R_\Psi x\| = \|x\|$ for any $x \in \mathbb{R}^n$. Then we have:

$$\begin{aligned} \|Lu - \lambda u\| &= \|R_\Psi(Lu - \lambda u)\| \\ \|Lu - \lambda u\| &= \|L(R_\Psi u) - \lambda(R_\Psi u)\| \end{aligned}$$

□

We have an even stronger statement of invariance for energy loss: **given a predicted set of k orthogonal vectors, rotating the vectors within the same subspace does not impact loss**. In other words, a model trained on energy loss only needs to predict the correct *subspace* of k eigenvectors. This is clearly not true of eigenvector loss. Depending on the application, this kind of invariance can be good or bad.

Lemma 3 (Energy loss is rotation invariant). *Let L be a Laplacian matrix and $V \subseteq \mathbb{R}^n$ be some k -dimensional subspace. Suppose $U = [u_1, u_2, \dots, u_k], W = [w_1, w_2, \dots, w_k] \in \mathbb{R}^{n \times k}$ are both orthonormal bases for V . Then we have:*

$$\frac{1}{k} \text{Tr}(U^\top L U) = \frac{1}{k} \text{Tr}(W^\top L W)$$

Proof. Note that $U U^\top = W W^\top$, as they are both orthogonal projectors for the same subspace. Then we have, by the cyclic property of trace:

$$\frac{1}{k} \text{Tr}(U^\top L U) = \frac{1}{k} \text{Tr}(U U^\top L) = \frac{1}{k} \text{Tr}(W W^\top L) = \frac{1}{k} \text{Tr}(W^\top L W)$$

□

A.4 Node feature augmentation

The diffusion operator P of a graph G is defined as:

$$P = D^{-1}A$$

Each entry P_{ij} represents the probability of starting a random walk at node i and ending at node j after one step. One can also take powers of the diffusion operator, P^t . Each entry of the powered matrix, P_{ij}^t , represents the probability of starting a random walk at node i and ending at node j after t steps

The j^{th} wavelet operator Ψ_j of a graph G is defined as:

$$\begin{aligned}\Psi_j &= P^{2^{j-1}} - P^{2^j} \\ \Psi_0 &= I - P\end{aligned}$$

A wavelet bank, \mathcal{W}_J is a collection of wavelet operators such that:

$$\mathcal{W}_J = \{\Psi_j\}_{0 \leq j \leq J} \cup P^{2^J}$$

Wavelet positional embeddings encode information about the relative position of each node within the graph. We randomly select two nodes from each graph, i and j , and start dirac signals δ_i, δ_j . We then apply these signals to each wavelet, Ψ_k , in our wavelet bank. The wavelet positional embedding for node m is the m^{th} row of the resulting matrix.

$$\begin{aligned}w_{m,k} &= \Psi_k(m, \cdot) \begin{bmatrix} | & | \\ \delta_i & \delta_j \\ | & | \end{bmatrix} \\ w_m &= [w_{m,1} \quad \dots \quad w_{m,J}]\end{aligned}$$

Diffused dirac embeddings encode information about the connectedness of each node and its neighbors. For each node, m , we apply the m^{th} row of the diffusion matrix P to each wavelet Ψ_k in our wavelet bank. As above, the difused dirac embedding for node m is the m^{th} row of the resulting matrix.

$$\begin{aligned}d_{m,k} &= \Psi_k(m, \cdot) P(m, \cdot)^\top \\ d_m &= [d_{m,1} \quad \dots \quad d_{m,J}]\end{aligned}$$

Lemma 4 (Uniqueness up to co-spectrality). *Let G_1, G_2 be graphs of size n with Laplacian matrices L_1, L_2 respectively. Let d_m^1, d_m^2 represent the diffused dirac embeddings for each node in G_1, G_2 . Then if L_1 and L_2 have different eigenvalues, $\{d_m^1 : m \leq n\} \neq \{d_m^2 : m \leq n\}$*

Proof. Consider the random-walk Laplacian of a graph: $L_{rw} := I - D^{-1}A = I - P$. Moreover, note that $L_{rw} = D^{-1}L$. Observe that

$$\begin{aligned}L_{rw}Dv &= D^{-1}LDv \\ &= D^{-1}U\Lambda U^\top Dv \\ &= Bv \text{ for some diagonalizable matrix } B \text{ with eigenvalues } \lambda_1, \dots, \lambda_n\end{aligned}$$

Where $U = [\psi_1 \quad \dots \quad \psi_n]$, with ψ_i orthonormal eigenvectors of L and Λ is the diagonal matrix of eigenvalues $\lambda_1, \dots, \lambda_n$ of L . Any change to the eigenspectrum of L , clearly results in a change to L_{rw} , and therefore P . Since $\Psi_0 = I - P$, any two graphs with distinct Laplacian eigenspectra will have distinct diffused dirac node embeddings. \square

A.5 Detailed experimental settings

A complete overview of model hyperparameters and settings can be found in Table 4. Heuristically, the Graph-level MLP head hidden dimension is chosen to be the max # nodes multiplied by the hidden dimension size of the base GNN. We do NOT omit the trivial eigenvector when counting number of eigenvectors predicted.

Table 4: A comprehensive list of all model hyperparameters used during the eigenvector pre-training step. All hyperparameters highlighted in gray are specific to eigenvector-learning, while other listed configs reflect general GNN settings (and are set to match default values in each respective baseline work).

Method	GIN (4.1)	GIN (4.1)	GIN pre-training (4.2)	GPSE (4.3)
Pre-training dataset	ZINC-12k	QM9 (134k)	ZINC15 (2M), ChEMBL (456K)	MolPCBA (324K)
Base architecture	GIN	GIN	GIN	MPNN
# params	33543	32883	2252210	22075899
# layers of per-node feature update	3	3	2	1
# layers of message passing	4	4	5	20
Hidden dim	60	60	300	512
Activation fn	ReLU	ReLU	ReLU	ReLU
Dropout	0.1	0.1	0.2	0.2
Batch size	128	128	32	1024
Learning rate	0.001	0.001	0.001	0.005
Optimizer	Adam	Adam	Adam	AdamW
Scheduler	ReduceLROnPlateau	ReduceLROnPlateau	None	CosineWithWarmup
	patience=5, factor=0.9	patience=20, factor=0.5	-	-
Pre-Training Epochs	200	100	100	120
Fine Tuning Epochs	500	150	100	-
Laplacian norm type	Unnormalized	Unnormalized	Unnormalized	Symmetric
# eigenvectors predicted	6	6	5	5
Initial features	Diffused dirac + Wavelet pos.	Diffused dirac + Wavelet pos.	Molecule features	Random
MLP head type(s)	Graph-level	Graph-level	Graph-level, per-node	Graph-level, per-node
Graph-level MLP max # nodes	40	40	50	50
MLP head # layers	5	5	1	2
MLP head hidden dim	2400	2400	N/A	1600, 32
MLP head activation fn	ReLU	ReLU	N/A	ReLU
Loss function (and coefficient)	2*Eigenvector + 1*energy	2*Eigenvector + 1*energy	0.25 * Eigenvector + 0.05 * ortho	0.25 * Eigenvector
Other features/notes		Removed graphs with less than six nodes during pre-training		Residual gating, virtual node

A.6 Modifying existing pre-training method

A.6.1 Learning rate tuning

We keep the majority of the settings from [3] the same. For downstream fine-tuning, we tune over 7 learning rates for fair comparison according to [4]. We run each method and learning rate over 3 seeds, and select the learning rate based on mean validation accuracy over all learning rates.

A.6.2 Downstream datasets

We briefly list and cite the five downstream datasets here for reference. The five datasets are the datasets chosen in [4], and are a subset of the eight primary downstream datasets evaluated in [3].

- **BACE:** Qualitative binding results [19]
- **BBBP:** Blood-brain barrier penetration [20]
- **Tox21:** Toxicity data [21]
- **Toxcast:** Toxicology measurements [22]
- **SIDER:** Database of adverse drug reactions (ADR) [23]

A.7 Modifying existing graph structural encoder

A.7.1 Loss function comparison

We claim that the sum of MAE and cosine similarity loss used in [1] is ill-posed for learning eigenvectors.

To address sign ambiguity, the original GPSE model only learns the absolute value of each Laplacian eigenvector as its target. This improves performance over training without absolute value, but two shortcomings still arise. This (1) provides strictly less information than learning the true eigenvectors, and (2) does not capture basis ambiguity, making it ill-posed for eigenvectors with higher multiplicity (or eigenvectors with small eigengaps).

We demonstrate this claim experimentally in Figure 2. We train the default GPSE settings and architecture using (1) eigenvector loss (ours), and the default cosine similarity + MAE loss (GPSE). We train for 600 epochs on 1% of the MolPCBA dataset and plot eigenvector and energy losses per-epoch. We also plot the loss when outputting random orthogonal vectors for comparison. While training on cosine similarity + MAE achieves better-than-random results, sign and basis ambiguity issues severely limit the model’s ability to learn meaningful eigenvectors.

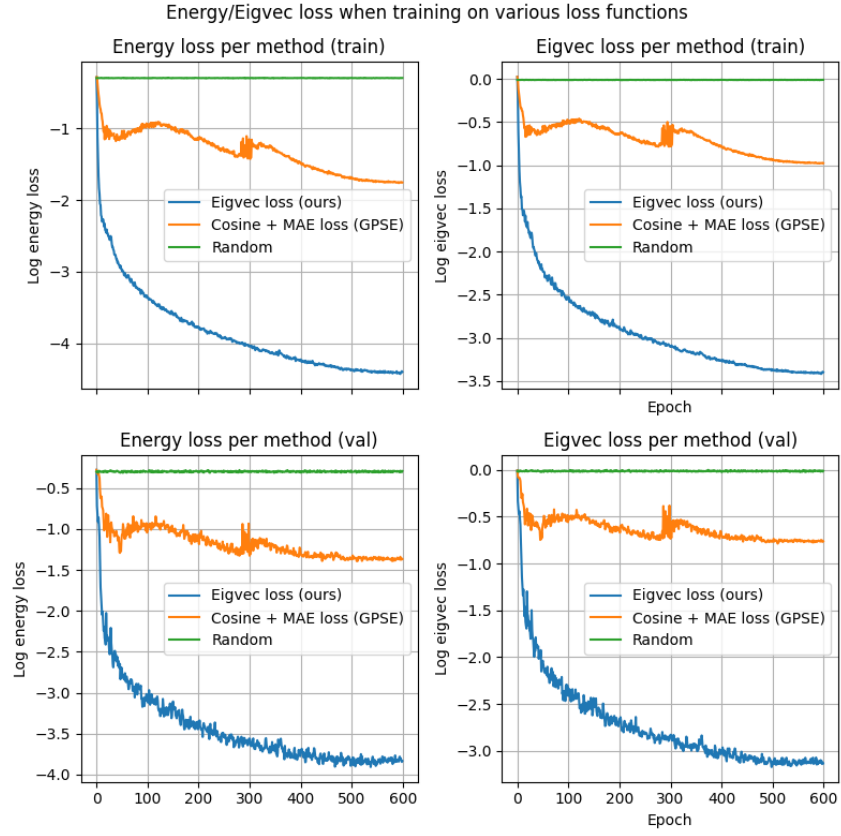


Figure 2: A comparison of energy loss and eigenvector loss, when the GPSE architecture is trained on (1) eigenvector loss (ours), (2) cosine similarity + MAE [1], and (3) no loss (outputting random vectors). All losses displayed are in natural log scale for visual purposes.